Impact of Operational Parameters on Single Beamlet Deflection in a Negative Ion Source for NBI Applications

Andrew Hurlbatt,[a)] Federica Bonomo, Guillermo Orozco, Riccardo Nocentini, Christian Wimmer, and Ursel Fantz

Max-Planck-Institut für Plasmaphysik, Boltzmannstrasse 2, 85748 Garching, Germany

[a)]*Corresponding author: andrew.hurlbatt@ipp.mpg.de*

Abstract. For current and future large scale tokamaks, neutral beams for heating and current drive are generated from the neutralisation of large negative ion beams with energies up to 1 MeV and current of up to 40 A. To improve efficiency and prevent high heat loads on beamline components, permanent magnets are used to deflect co-extracted electrons out of the beam at a low energy. This field also affects the negative ions as they are accelerated, causing beamlets to exit the grid system with a residual offset and deflection angle. This adversely affects the overall divergence of the beam, and compensation is foreseen in future devices. Measurements of the residual deflection of a single beamlet have been carried out at the BATMAN Upgrade test facility by calculating relative beamlet angles from beam emission spectroscopy (BES) spectra, and through the use of one-dimensional carbon fibre composite (1D-CFC) tile calorimetry to find beamlet positions. It is described how these measurements can be made, and that they are limited to relative measurements only, for a single beamlet and for a single line of sight. The amount of beamlet deflection is shown to change significantly, by up to 0.6° (10 mrad), depending on the operational parameters used. As is to be expected the beamlet deflection angle is observed to be affected by changes to the voltages of the acceleration system. However, the beamlet deflection angle is also observed to change with RF power and other source parameters, which, to a first approximation, should only affect beamlet divergence, and not the deflection. These changes to beamlet deflection through parameters other than the grid voltages used may have consequences for systems planning to use suppression systems for the zig-zag deflection. The effectiveness of the suppression system may be reduced due to changes in the source parameters, which could lead to beam losses and high heat loads on downstream components.

INTRODUCTION

The next generation large-scale tokamak ITER will require large amounts of power for heating and current drive, for which neutral beam injection (NBI) is foreseen to play a major role. ITER will have two NBI systems, each generating up to 16.5 MW of neutral beam heating and current drive from 40 A of precursor negative hydrogen or deuterium ion beams, upon which strict requirements are placed [1, 2, 3]. In order to minimise transmission losses and reduce power loads on beamline components, the component beamlets, of which there are 1280, are required to have a 'core' divergence of no more than 7 mrad, with an allowable 30 mrad 'halo' component carrying up to 15% of the beam power.

To create such a beam, future devices and current test facilities generate an RF driven hydrogen (or deuterium) plasma, which expands through a magnetic filter field, designed to reduce the electron temperature from around 10 eV to roughly 1 eV. This is to avoid destruction of the required negative hydrogen ions which are mainly produced by surface conversion of atomic hydrogen on caesiated surfaces within the source. On the other side of this filter field is a multi-grid electrostatic extraction and acceleration system, with potentially hundreds of individual apertures each creating a single 'beamlet', the combination of which forms the whole ion beam. This grid system consists of a plasma grid (PG), extraction grid (EG), zero or more acceleration grids, and a final grounded grid (GG). As electrons are inevitably co-extracted along with negative ions, permanent magnets are embedded between aperture rows in the EG to create a magnetic field perpendicular to the beam direction, the strength of which is sufficient to deflect electrons out of the beam to impact on the surface of the EG. These magnets alternate row-wise in polarity, so the residual horizontal deflection of the ion beamlets alternates left and right between beamlet rows to create a zig-zag effect. The use of additional permanent magnets in the EG for suppression of this zig-zag deflection has been tested at some facilities [4, 5], and is foreseen at MITICA and the ITER injectors [6, 7], for which horizontal beam misalignment must be less than 2 mrad [8].

One test facility which is investigating effects important for the next generation of devices is the BATMAN Upgrade test facility (BUG), which is described in detail in previous publications [9, 10]. Important details on the plasma source, beyond what is described above, are that the plasma is generated by inductive coupling of up to 150 kW of RF power, the magnetic filter field is generated by a DC current (I_{PG}) of up to 3 kA flowing vertically through the PG, and that the PG can be biased positively relative to the source body by means of a constant current supply (I_{Bias}). Each

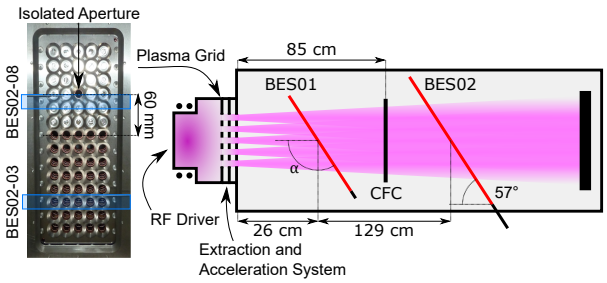

FIGURE 1. Sketch of the ion source at BUG, showing the masking of the PG and the location of the main beam diagnostics.

grid in the system contains 70 apertures in total, in 14 rows of 5 columns. For the data given in this work, the top 7 rows of apertures in the PG were closed, with the exception of a single aperture in the middle of the fourth row, as shown on the left of Figure 1. Two voltages are defined for the grid system: U_{extr} is the voltage between the PG and the EG, and U_{acc} is between the EG and GG.

Results from two types of beam diagnostics will be presented in this work. The first is beam emission spectroscopy (BES) which observes Doppler shifted H_α emission coming from the interaction of the beam particles with background gas downstream of the grid system. By analysing the shape of the Doppler shifted peak, one can determine properties of the velocity distribution of the beam particles, including a divergence for the beam [11, 12, 13, 14]. In BUG there are two BES systems - BES01 with 5 lines of sight located 26 cm from the GG, and BES02 with 11 lines of sight at 129 cm. In both systems, lines of sight observe horizontally, and are numbered bottom to top; for example, BES02-03 observes the lower group of beamlet rows, whereas BES01-04 and BES02-08 both collect light from the isolated beamlet. The second beam diagnostic is a newly installed 1D carbon fibre composite (CFC) tile that can be used to intercept the beam. The highly directional thermal conductivity of the tile allows the rear side to be observed by an IR camera (FLIR A655SC) to obtain an image of the beam hitting the front side, providing a measure of the distribution of particles within a beamlet. The location of these diagnostics relative to the grid system is sketched in Figure 1.

Both of these diagnostics are primarily used to investigate the divergence of the ion beams, with a focus on the isolated beamlet in order to exclude the effect of the zig-zag deflection. In this work, the same raw data is analysed in a different manner to investigate the deflection of beamlets caused by this zig-zag deflection.

MEASURING BEAMLET DEFLECTION ANGLES

The working principle of BES uses the equation for relativistic Doppler shift, given in Equation 1, where λ_D and λ_0 are the Doppler shifted and unshifted wavelengths, respectively, β is the ratio of the speed of the emitting object to that of light, γ is the Lorentz factor, and α is the observation angle, relative to the direction of travel of the emitting object.

$$\lambda_D = \lambda_0 \gamma (1 + \beta \cos \alpha) \tag{1}$$

By knowing the observation angle α, and given measurements of U_{extr} and U_{acc}, one is also able to calculate γ and β, and thereby the expected λ_D. The Doppler peak measured from the isolated beamlet using BES02-08 is shown in Figure 2 for different values of RF power. In an experiment where only RF power is changed, one would expect that the extracted ion current increases with power. This will change the normalised perveance (P/P_0), which is proportional to ${U_{extr}}^{-3/2}$, total extracted current I_{extr}, and the dimensions of the grid system, and normalised to P_0, which is the maximum perveance as predicted by the Child-Langmuir law. This quantity describes how the beamlet interacts with the first electrostatic lens. If the normalised perveance changes, then the measured divergence is expected to be affected, which is observed in Figure 3(a), which also demonstrates the difference between the measured divergence for a single beamlet and that for a group of beamlets. The differences between the spectra for a single or a group of beamlets is demonstrated in Figure 3(b). However, in addition to this, the Doppler peaks in Figure 2 are seen to differ from λ_D, and this difference changes depending on the RF power in a regular and repeatable manner.

For calculation of the divergence, a Gaussian function is fitted to the top 70% of the Doppler peak, the width of which is related to the spread in particle angles and therefore the divergence. The difference between the central

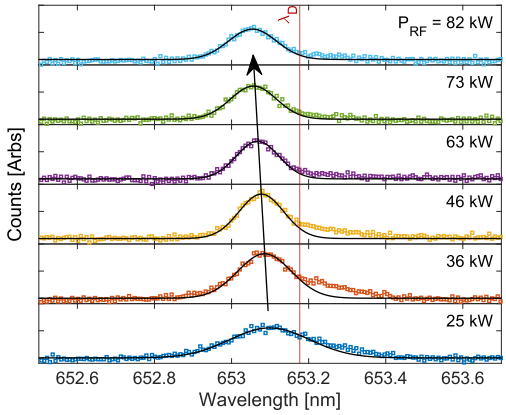

FIGURE 2. Zoomed in spectra showing the Doppler peak measured by BES02-08 of the single beamlet for a variation in RF power. Data points are given as squares, and a Gaussian fit to the top 70% of the Doppler peak is plotted as a line over each spectrum. Source filling pressure was 0.5 Pa, U_{extr} and U_{acc} were 4.6 kV and 31.3 kV respectively, I_{PG} was 780 A, and I_{Bias} was 4.3 A. The vertical line labelled λ_D is the value calculated from Equation 1, using the unshifted wavelength of H_α 656.279 nm.

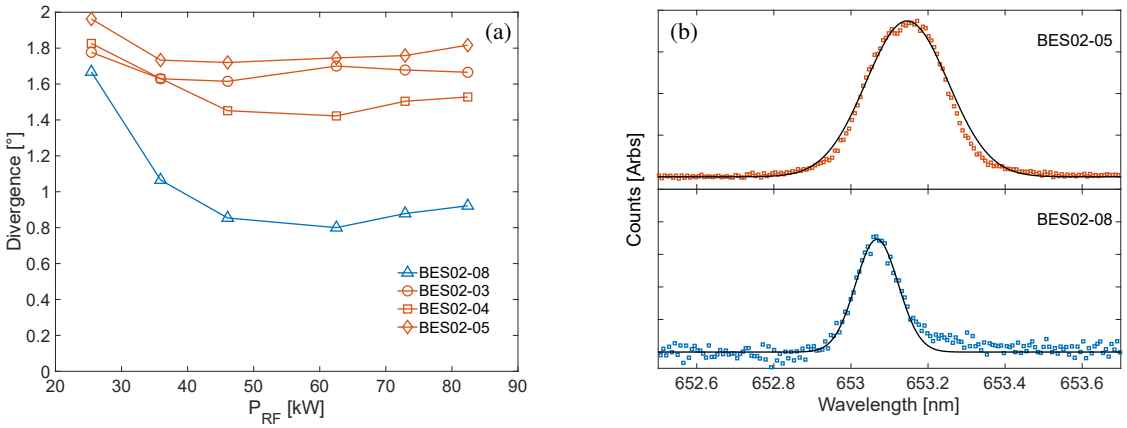

FIGURE 3. (a) Calculated divergence as a function of RF power for the isolated beamlet, using BES02-08, and three other lines of sight observing groups of beamlets. Parameters are the same as for Figure 2. (b) Example spectra for the case at 63 kW from BES02-08 (bottom) observing the single beamlet and BES02-05 (top) observing multiple rows of beamlets.

wavelength of this Gaussian fit (hereon referred to as the measured Doppler wavelength, $\lambda_{D,M}$), and the expected value of λ_D is plotted for four lines of sight in Figure 4. BES02-08 corresponds to the isolated beamlet, whereas BES02-02, BES02-03, and BES02-04 collect light from multiple beamlet rows [15], and are separated vertically by 3 cm. The behaviour of $\lambda_D - \lambda_{D,M}$ is different for each line of sight, as are the average values over the parameter range plotted. Errors in this method of evaluation could come from uncertainty in either the observation angle or the beam energy. An error in the observation angle of a line of sight would mean a non-zero central value for $\lambda_D - \lambda_{D,M}$ for that particular line of sight, but this offset would be constant, as the lines of sight are fixed in position. Measurement errors in U_{extr} or U_{acc} would lead to an identical offset for all lines of sight. A different $\lambda_{D,M}$ could also be caused by differences in the mixing of beamlets, leading to changes in the ratio of light collected from right- and leftward deflected beamlets. None of these potential sources of error can explain the behaviour of $\lambda_D - \lambda_{D,M}$ for BES02-08, leaving changes in the average angles of observed particles - beamlet deflection - as the only explanation. Although the deflection of the beamlets observed by the other lines of sight in Figure 4 is likely also changing, this behaviour is masked by the mixing of Doppler peaks from rows with alternating deflection. A changing of this mixing as beamlet divergence changes [15], as seen in Figure 3, means that the behaviour for lines of sight observing multiple beamlets is too complex to understand fully with the available experimental data.

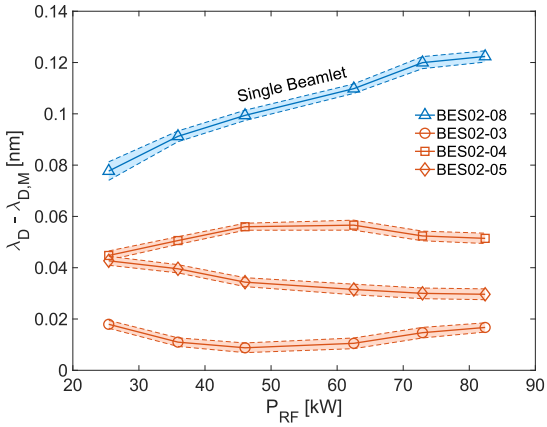

FIGURE 4. The evaluated difference between the wavelengths of the measured Doppler peak and the expected λ_D as a function of RF power for the isolated beamlet, using BES02-08, and three other lines of sight observing groups of beamlets. Parameters are the same as for Figure 2. The 1-σ confidence interval that results from the Gaussian fitting to the Doppler and unshifted peaks is given as bands around each line.

By assuming beamlets are deflected by an additional angle of ϕ, one can define an expression for $\lambda_{D,M}$ as given in Equation 2. By subtracting Equation 1 from this, one arrives at an expression for the angle ϕ as given in Equation 3.

$$\lambda_{D,M} = \lambda_0 \gamma (1 + \beta \cos(\alpha + \phi)) \tag{2}$$

$$\phi = \arccos\left[\frac{\lambda_{D,M} - \lambda_D}{\lambda_0 \gamma \beta} + \cos\alpha\right] - \alpha \tag{3}$$

The possible errors from the observation angle, the high voltage measurement, and beamlet mixing should not be ignored, and restrict the applicability of Equation 3 to comparing relative changes for a single beamlet and a single line of sight.

CHANGES TO BEAMLET DEFLECTION ANGLE

In the simplified picture used to create Equation 3, the RF power delivered to the plasma should not have any effect on the horizontal deflection of beamlets. However, as well as affecting the extracted ion current, changes in the plasma density near the PG can cause changes to the shape of the meniscus [16]. This could, in turn, affect both the radial distribution of ions within the beamlet, and the trajectories of the ions during the initial beamlet formation, as shown by the changes to the divergence given in Figure 3. Changes to either of these will impact the magnetic fields that are experienced by the ions, and thereby the beamlet deflection.

In contrast to the RF power, altering the grid voltages can be expected to change the beamlet deflection, as has been previously shown on a tungsten wire calorimeter at BUG [10]. Neglecting relativistic effects, the motion of particles undergoing acceleration through the grid system is determined by the Lorentz force, given in Equation 4. The angle of a particle is defined as $\arctan v_\perp / v_\parallel$; given the field orientation during acceleration and the small angles involved, $v_\perp$ can be approximated as the integral over time of the cross product of particle velocity $\boldsymbol{v}$ and the magnetic field experienced by the particle, $\boldsymbol{B}$, as given in Equation 6.

$$m\boldsymbol{a} = q\boldsymbol{E} + q\boldsymbol{v} \times \boldsymbol{B} \tag{4}$$

$$\Delta\boldsymbol{v} = \frac{q}{m}\int \boldsymbol{E} + \boldsymbol{v} \times \boldsymbol{B}\mathrm{d}t \tag{5}$$

$$\Delta v_\perp \approx \frac{q}{m}\int \boldsymbol{v} \times \boldsymbol{B}\mathrm{d}t \tag{6}$$

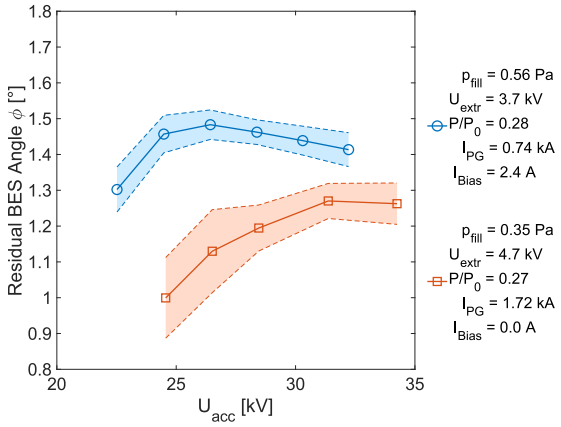

FIGURE 5. Behaviour of the angle ϕ from BES02-08 as a function of U_{acc} for two scans with different experimental parameters, as given in the figure. In this plot, and those following, the deflection axis does not start at zero. This is due to the caveat of not being able to detect offset errors in the results.

The magnetic field $\boldsymbol{B}$ is fixed in space, but varies within the aperture, as indicated in a previous publication [17]. As a first level of approximation, changes in grid voltages will mean that particles reach places in space with different velocities, thereby changing the integral of $\boldsymbol{v} \times \boldsymbol{B}$. In addition, changes to the shapes of electrostatic lenses will put particles on different trajectories through the aperture, changing the magnetic field they experience. Both of these effects mean that changes to the grid voltages will impact the net beamlet deflection.

A consequence of this can be seen in Figure 5, which shows how this calculated beamlet deflection angle ϕ varies as a function of U_{acc} for two different scans, where other parameters were held constant. In both cases, there is a clear influence of U_{acc} on the beamlet angle, but the behaviour is different for the different scans. Although the change with U_{acc} is expected to occur, the analysis of Equation 6 performed above is not able to say exactly what those changes should be, and so an explanation for the trends - in particular the apparent turning points - is not yet clear. Between the two scans, the source filling pressure p_{fill}, U_{extr}, I_{PG}, and I_{Bias} all change. This implies that other source parameters also affect the beamlet deflection, and that the particle distributions are different before passing into the second electrostatic lens. The analysis presented in this work has been performed on existing experimental data; more detailed investigations are required to explore these effects.

Figure 6 gives the changes in beamlet angle for three scans in total high voltage $U_{HV} = U_{acc} + U_{extr}$, which were performed with a constant ratio between U_{acc} and U_{extr} of 6.8. The normalised perveance (P/P_0) was also kept constant. Maintaining these two parameters constant should, in an idealised picture, prevent the beam optics from changing. This is confirmed by only small changes to the beamlet divergence as measured by BES02-08 (not shown), with a variation of around 0.1° from the mean value, which is 1.3° for scan 1, and 1.0° for scans 2 and 3. Despite this roughly constant divergence for each of the scans, variations to U_{HV} still have a relatively large impact on the beamlet deflection, with changes up to 0.5° in the extreme case for scan 3.

The trends with U_{HV} lie on top of effects caused by changes to the other experimental parameters, as evidenced by the differences between the three scans. Curves 2 and 3 differ mainly by an offset, which could stem from their differences in p_{fill}, I_{PG}, or I_{Bias}. Curve 1 additionally differs from the others in the qualitative behaviour. Comparing Figures 5 and 6, it can be seen that the range of beamlet angles is significantly higher for variations in U_{HV} than in U_{acc}, by a factor of around 2. In Figure 6, curve 3 shows the maximum variation in deflection for a single scan, with a range of around 0.6°. In Figure 5 the maximum variation for a single scan is only around 0.3°. A possible reason for this difference could be the changes that are made to U_{extr} as part of the scans in Figure 6. As the ions are moving slower in the PG – EG gap than in subsequent gaps, changes to the experienced magnetic field would have greatest impact here.

As mentioned previously, BUG has recently been upgraded with a CFC target for beamlet imaging. Although work is still ongoing for how best to determine the beamlet shape from the images obtained, the centre of the beamlet can be easily measured with a sub-mm accuracy. However, as with the BES diagnostic, uncertainties in alignments mean that it is not possible to obtain an absolute position for the beamlet with the same level of accuracy. One should also bear in mind that the BES diagnostic is a measure of the velocity distribution, whereas the CFC target measures position

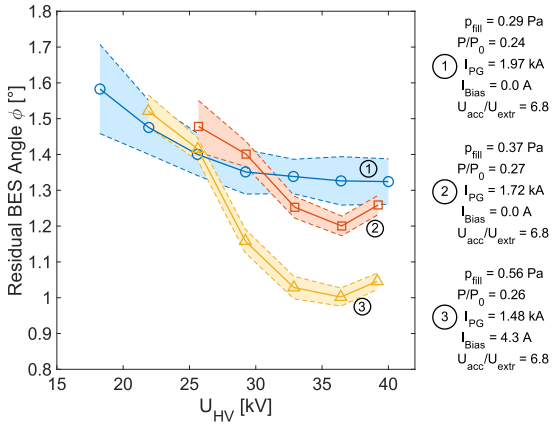

FIGURE 6. Behaviour of the angle ϕ from BES02-08 as a function of U_{HV} for three scans with the same ration of U_{acc}/U_{extr} = 6.8, but different other experimental parameters, as given in the figure.

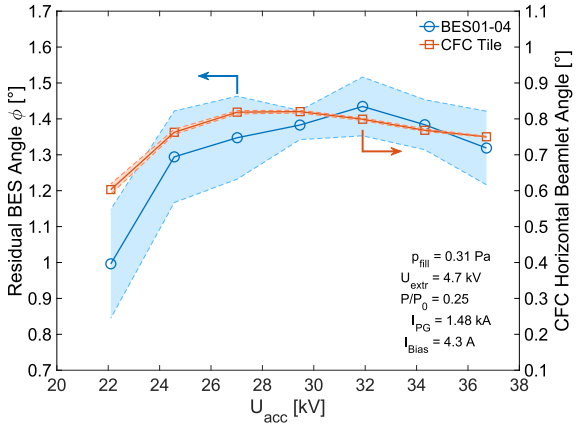

FIGURE 7. Comparison of the angle ϕ from BES01-04 with the horizontal angle calculated from the CFC target for a scan in U_{acc}. Both lines have bands showing the 1-σ confidence interval that results from the numerical fitting.

only. In a given direction, the positional and velocity particle distribution distributions for each beamlet will be highly correlated. However, beamlets do not travel straight through the middle of the aperture during formation, due to the deflection field, so there are still possibilities for changes to the apparent origin of the beamlet.

With these caveats, Figure 7 shows a comparison between the angle ϕ evaluated from BES01-04 and the horizontal angle of the beamlet calculated using the CFC target, assuming that the beamlet origin is the centre of the aperture. The confidence interval plotted for the BES results shows only the uncertainty resulting from Gaussian fits to the Doppler and unshifted peaks in the observed spectra, which is lowest when the signal-to-noise ratio is high. Both vertical axes represent a range of 1° of deflection. This data shows that there is an excellent agreement for the motion of the beamlet between the two diagnostics, despite their fundamental differences. There is a small difference in the range of the deflection change that is observed, which may be due to the difference in measurement type explained in the previous paragraph. The difference in offset may be due to any of the previously mentioned uncertainties in alignments. In comparison with the other U_{acc} scans in Figure 5, the behaviour is observed to be different again, but this difference cannot yet be pinned down to any particular change in experimental parameters.

CONCLUSIONS

Using BES to obtain a relative measure of beamlet deflection provides a non-invasive way of measuring changes in the beamlet angle, that agrees with CFC measurements of the same. As is discussed in previous sections, these measurements come with caveats on their applicability, namely their restriction to relative changes for a single beamlet observed by a single line of sight. This is due to possible offset errors introduced through high voltage measurements or misaligned observation optics.

Despite only relative measurements being available, the data obtained using BES is sufficient to say with confidence that the amount of horizontal deflection of a single beamlet in BUG is affected by changes in operational parameters. This includes not only expected influences due to grid voltages, but also unexpected ones due to RF power, and some combination of p_{fill}, I_{PG}, and I_{Bias}. This is clear to see particularly in Figure 6, where points with the same U_{HV}, and thereby same U_{acc} and same U_{extr}, differ in beamlet deflection by up to 0.25°.

Despite the present experimental data not being sufficient to explain or fully characterise the behaviour of the horizontal beamlet deflection, this work shows that it can vary in unexpected ways. The most likely explanation for this is that changes in the plasma properties lead to differences in the shape of the meniscus, the boundary between the plasma and the region where fields of the extraction system dominate. These differences are then observed as a change to the beamlet deflection angle. This may have consequences for ion sources that are designed with suppression systems for the zig-zag deflection, as the suppression may be reduced in effectiveness, leading to an underestimation of downstream losses and heat loads on components. There are also possible consequences for comparisons of data between different ion sources, and between experiments and simulations. When comparing result between sources, both with and without compensation, the deflection is likely to behave in different ways, which may cause difficulties in comparing results. Current beamlet simulations are not able to take detailed plasma physics into account, and are therefore liekly to miss changes to the deflection that are present in the experiment. It is clear that further systematic studies are needed to investigate the behaviours and trends of the horizontal beamlet deflection in more detail.

ACKNOWLEDGMENTS

This work has been carried out within the framework of the EUROfusion Consortium and has received funding from the EURATOM research and training programme 2014-2018 and 2019-2020 under grant agreement No. 633053. The views and opinions expressed herein do not necessarily reflect those of the European Commission.

REFERENCES

1. ITER, "Neutral beam heating and current drive system," (2011), Design Description Document (DDD) 5.3.
2. R. Hemsworth, H. Decamps, J. Graceffa, B. Schunke, M. Tanaka, M. Dremel, A. Tanga, H. P. L. de Esch, F. Geli, J. Milnes, T. Inoue, D. Marcuzzi, P. Sonato, and P. Zaccaria, "Status of the ITER heating neutral beam system," Nuclear Fusion **49**, 045006 (2009).
3. R. S. Hemsworth, D. Boilson, P. Blatchford, M. Dalla Palma, G. Chitarin, H. P. L. de Esch, F. Geli, M. Dremel, J. Graceffa, and D. Marcuzzi, "Overview of the design of the ITER heating neutral beam injectors," New Journal of Physics **19**, 025005 (2017).
4. M. Kashiwagi, M. Taniguchi, N. Umeda, M. Dairaku, H. Tobari, H. Yamanaka, K. Watanabe, T. Inoue, H. P. L. de Esch, L. R. Grisham, D. Boilson, R. S. Hemsworth, and M. Tanaka, "Compensations of beamlet deflections for 1 MeV accelerator of ITER NBI," AIP Conference Proceedings **1515**, 227 (2013).
5. G. Chitarin, A. Kojima, D. Aprile, P. Agostinetti, M. Barbisan, S. Denizeau, M. Ichikawa, J. Hiratsuka, M. Kashiwagi, N. Marconato, A. Pimazzoni, E. Sartori, G. Serianni, P. Veltri, and M. Yoshida, "Improving a negative ion accelerator for next generation of neutral beam injectors: Results of QST-consorzio RFX collaborative experiments," Fusion Engineering and Design **146**, 792–795 (2019).
6. G. Chitarin, P. Agostinetti, D. Aprile, N. Marconato, and P. Veltri, "Cancellation of the ion deflection due to electron-suppression magnetic field in a negative-ion accelerator," Review of Scientific Instruments **85**, 02B317 (2014).
7. M. Cavenago and P. Veltri, "Deflection compensation for multiaperture negative ion beam extraction: analytical and numerical investigations," Plasma Sources Science and Technology **23**, 065024 (2014).
8. H. de Esch, M. Kashiwagi, M. Taniguchi, T. Inoue, G. Serianni, P. Agostinetti, G. Chitarin, N. Marconato, E. Sartori, P. Sonato, P. Veltri, N. Pilan, D. Aprile, N. Fonnesu, V. Antoni, M. Singh, R. Hemsworth, and M. Cavenago, "Physics design of the HNB accelerator for ITER," Nuclear Fusion **55**, 096001 (2015).
9. B. Heinemann, M. Fröschle, H. D. Falter, U. Fantz, P. Franzen, W. Kraus, R. Nocentini, R. Riedl, and B. Ruf, "Upgrade of the BATMAN test facility for H- source development," AIP Conference Proceedings **1655**, 060003 (2015).
10. U. Fantz, F. Bonomo, M. Fröschle, B. Heinemann, A. Hurlbatt, W. Kraus, L. Schiesko, R. Nocentini, R. Riedl, and C. Wimmer, "Advanced NBI beam characterization capabilities at the recently improved test facility BATMAN Upgrade," Fusion Engineering and Design **146**, 212–215 (2019).

11. P. Franzen and U. Fantz, "Beam homogeneity dependence on the magnetic filter field at the IPP test facility MANITU," AIP Conference Proceedings **1390**, 310–321 (2011).
12. B. Heinemann, U. Fantz, W. Kraus, L. Schiesko, C. Wimmer, D. Wünderlich, F. Bonomo, M. Fröschle, R. Nocentini, and R. Riedl, "Towards large and powerful radio frequency driven negative ion sources for fusion," New Journal of Physics **19**, 015001 (2017).
13. M. Barbisan, F. Bonomo, U. Fantz, and D. Wünderlich, "Beam characterization by means of emission spectroscopy in the ELISE test facility," Plasma Physics and Controlled Fusion **59**, 055017 (2017).
14. B. Zaniol, "Error evaluation in the spectroscopic measurement of high power beam angular divergence," Journal of Quantitative Spectroscopy and Radiative Transfer **112**, 513–518 (2011).
15. A. Hurlbatt, N. den Harder, U. Fantz, and the NNBI Team, "Improved understanding of beamlet deflection in ITER-relevant negative ion beams through forward modelling of beam emission spectroscopy," Fusion Engineering and Design **153**, 111486 (2020).
16. S. Mochalskyy, D. Wünderlich, B. Ruf, U. Fantz, P. Franzen, and T. Minea, "On the meniscus formation and the negative hydrogen ion extraction from ITER neutral beam injection relevant ion source," Plasma Physics and Controlled Fusion **56**, 105001 (2014).
17. A. Hurlbatt, N. den Harder, D. Wünderlich, U. Fantz, and the NNBI Team, "The particle tracking code BBCNI for large negative ion beams and their diagnostics," Plasma Physics and Controlled Fusion **61**, 105012 (2019).